

Mechanism of Thioredoxin-Catalyzed Disulfide Reduction. Activation of the Buried Thiol and Role of the Variable Active-Site Residues

Alexandra T. P. Carvalho,[†] Marcel Swart,^{‡,§} Joost N. P. van Stralen,[‡] Pedro A. Fernandes,[†] Maria J. Ramos,^{*,†} and F. Matthias Bickelhaupt^{*,‡}

REQUIMTE, Departamento de Química, Faculdade de Ciências, Universidade do Porto, Rua do Campo Alegre, 687, P-4169-007 Porto, Portugal, and Theoretical Chemistry, Vrije Universiteit, De Boelelaan 1083, NL-1081 HV Amsterdam, The Netherlands

Received: October 30, 2007; In Final Form: November 30, 2007

Thioredoxins (Trx) are enzymes with a characteristic CXYC active-site motif that catalyze the reduction of disulfide bonds in other proteins. We have theoretically explored this reaction mechanism, both in the gas phase and in water, using density functional theory. The mechanism of disulfide reduction involves two consecutive thiol–disulfide exchange reactions, that is, nucleophilic substitutions at sulfur ($S_N2@S$): first, by one Trx cysteine–thiolate group (Cys-32) at a sulfur atom of the disulfide substrate and, second, by the other Trx cysteine–thiolate group (the buried thiol of Cys-35) at the sulfur atom of the first Trx cysteine. We have investigated the intrinsic nature of such $S_N2@S$ substitution using the simple $CH_3S^- + CH_3SSCH_3$ model and how it is affected by solvation in aqueous solution. Next, we have examined how the behavior of the elementary $S_N2@S$ steps changes in the more realistic enzyme–substrate model CGPC + CH_3SSCH_3 , which contains the active-site of Trx. In all model reactions, solvation turns the hypervalent trisulfide anion (i.e., the $S_N2@S$ transition species) from a stable complex into a transition state. Importantly, our analyses suggest that the deprotonation of the buried thiol (which is required before the latter can enter into the second $S_N2@S$ step) is done by the leaving group evolving from the first $S_N2@S$ step. Finally, molecular dynamics (MD) simulations, in the gas phase and in water, of CGPC, CGGC, and the corresponding wild-type Trx and P34G Trx show that the activity of the thioredoxin active-site motif (CXYC) is determined not only by the structural rigidity associated with the particular variable residues (XY) but also by the number of amide N–H groups. The latter are involved in the stabilization of the Cys-32 thiolate and thus affect the acidity and nucleophilicity of this residue.

1. Introduction

Thioredoxin (Trx) is a ubiquitous redox enzyme that is involved, among others, in the reduction of cytoplasmatic proteins, for example, in the NADPH-fueled reduction of ribonucleotide diphosphates (rNDP), as illustrated in Scheme 1.^{1,2}

Thioredoxin belongs to the thioredoxin structural family of enzymes. The latter display a range of reduction potentials and hence fulfill various different functions ranging from reductases, such as thioredoxin (Trx) and glutaredoxin (Grx), to oxidases, such as disulfide bond formation A (DsbA) but also isomerases such as protein disulfide isomerase (PDI). Interestingly, these enzymes are structurally very similar. They all contain at least one domain with a characteristic thioredoxin fold. Also, they share a conserved stretch of sequence in the active site that contains a CXYC motif, where C stands for cysteine and XY are two variable residues.^{1,2} The XY residues of Trx are a glycine and a proline, of Grx a proline and a tyrosine, of PDI a glycine and a histidine and, finally, of DsbA a proline and a histidine.

Despite the important role of thioredoxin (vide supra), some key aspects of its catalytic mechanism remain unknown. The

available experimental data are mainly structural. On the basis of X-ray structures of reduced and oxidized thioredoxin enzymes, Holmgren et al.³ proposed a mechanism for redox reactions between two thioredoxins which has been extrapolated to other thioredoxin-catalyzed processes (see Scheme 2). First, the oxidized substrate (which contains a disulfide bond) binds noncovalently to the hydrophobic surface of the active Trx which is in its reduced state. Then, the Cys32 thiolate of Trx nucleophilically attacks a disulfide sulfur atom of the substrate ($S_N2@S$), leading to the formation of the so-called mixed disulfide intermediate in which the enzyme and substrate are covalently bound via a new disulfide bridge. Next, the Cys35 thiol group of the originally reduced Trx is deprotonated. This initiates a second $S_N2@S$ step in which the Cys35 thiolate attacks the Cys32 sulfur atom involved in the disulfide bridge, causing the rupture of the latter and the release of the products, i.e., an oxidized enzyme and a reduced, dithiol substrate.

An important issue in the above mechanism is the deprotonation of the cysteine thiol groups which activates them for $S_N2@S$ substitution. Previously, we have presented evidence that the nucleophilic cysteine in reduced Trx (i.e., Cys32) is deprotonated by water due to its low pK_a resulting from microdipoles of the α helix that point toward and, in this way, stabilize the thiolate⁴ (and not due to proton sharing between the two active-site cysteines).⁵

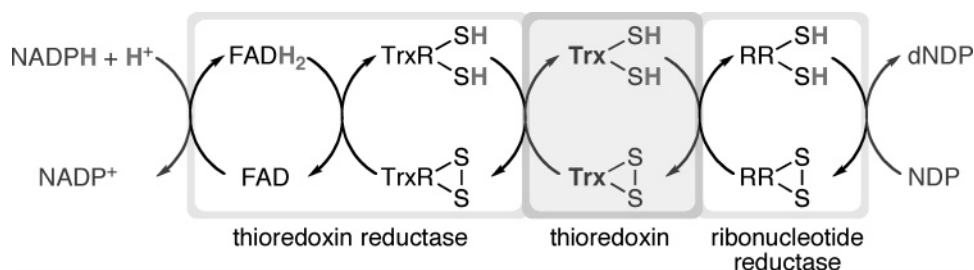
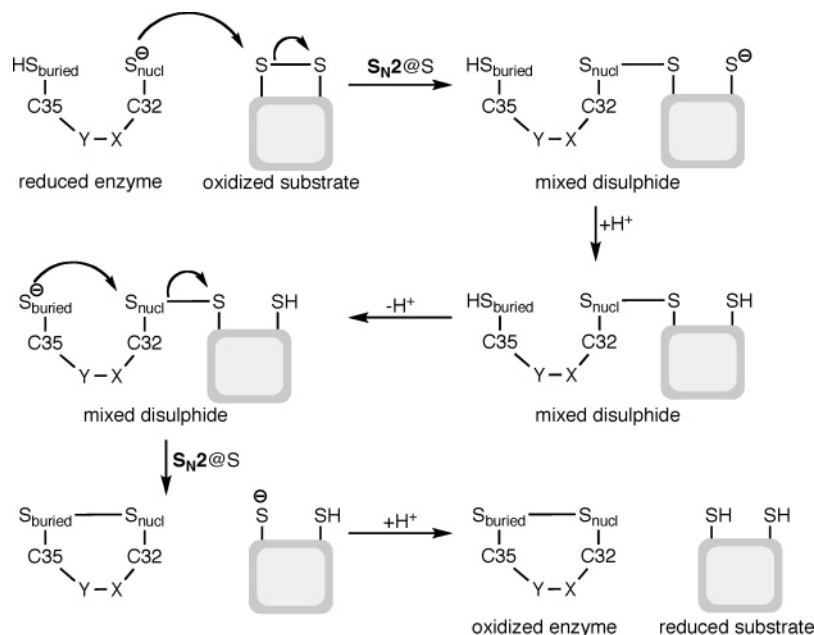
However, the mechanism through which the buried Cys35 is deprotonated and activated to perform the intramolecular

* Corresponding authors. E-mail: M.J.R., mjramos@fc.up.pt; F.M.B., fm.bickelhaupt@few.vu.nl.

[†] Universidade do Porto.

[‡] Vrije Universiteit.

[§] Present address: Institutió Catalana de Recerca i Estudis Avançats (ICREA), E-08010 Barcelona, Spain, and Institut de Química Computacional, Universitat de Girona, Campus Montilivi, E-17071 Girona, Spain.

SCHEME 1: Role of Trx in the NADPH-Driven Reduction of Ribonucleotides (NDP)**SCHEME 2: Mechanism of Trx-Catalyzed Reduction of Disulfide Bonds**

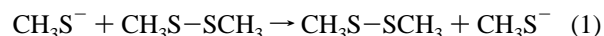
nucleophilic attack on Cys32 is still unknown. One hypothesis is that Asp26 is responsible for deprotonation of Cys35 because Asp26 is conserved in all thioredoxins and because of its proximity to the active-site cysteines.⁶ The main problem with this hypothesis is that Asp26 and Cys35 are still more than 6 Å apart. To explain the unlikely process of a proton transfer between such distant residues, Menchise et al.⁷ proposed that the transfer of the proton could be mediated by a water molecule.

Another issue is the question whether the $S_N2@S$ reactions involved in the thioredoxin-catalyzed reduction of disulfides proceed via a central barrier with a trisulfide transition state or without a central barrier, that is, via a single-well PES featuring a stable trisulfide intermediate. Nucleophilic substitution at third-period atoms (silicon, phosphorus, sulfur) generally proceed via a stable hypervalent transition complex, at variance with nucleophilic substitution at second-period atoms (carbon, nitrogen) which is characterized by a central barrier and a transition state.^{8–15} In particular, Bachrach and co-workers showed that replacing the hydrogen atom at the central sulfur atom of a thiol–disulfide reaction system by a methyl substituent leads to the occurrence of a pre- and post-TS that separate the stable trisulfide intermediate from reactant (RC) and product complexes (PC).^{8,9} This finding has been confirmed more recently by Fernandes and Ramos for larger systems such as methylthiolate reacting with the cyclic substrate dithiothreitol (DDT).¹⁶

In the present study, we aim at computationally exploring and clarifying the reaction mechanism of the Trx-catalyzed reduction of disulfides using the generalized gradient approximation (GGA) of density functional theory (DFT)^{17–23} and

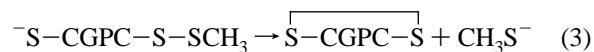
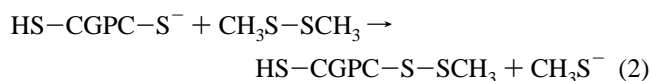
classical molecular dynamics (MD).²⁴ In particular, we address the issue of how the buried thiol is deprotonated and thus activated for the second $S_N2@S$ step. But we also examine the nature of the elementary $S_N2@S$ reactions (i.e., single-well, double-well, triple-well or unimodal reaction profile) and how they are affected by solvation in aqueous solution. The solvent is described by a continuum model (COSMO) and by discrete solvent molecules including counterions in the DFT and MD calculations, respectively (see Methods).

Thus, we have investigated three sets of model reaction systems. First, we examine the archetypal thiol–disulfide exchange reaction between methylthiolate and dimethyl disulfide (see eq 1). This serves to reveal the intrinsic nature (i.e., in the



absence of the protein) of sterically only slightly hindered thiol–disulfide and how this is affected by solvation. Furthermore, we use this model reaction to compare the performance of two GGA functionals: OPBE and BP86 (see Methods).

Second, we explore and analyze the two-step reduction of dimethyl disulfide by the full (hydrogen-terminated) active-site moiety of Trx (see eqs 2 and 3). These explorations lead to a



detailed insight into the two-step reaction mechanism. Here, we anticipate that evidence is obtained for a new mechanism for deprotonation and activation of the buried cysteine to initiate the second $S_N2@S$ step.

Third, we augment the above quantum chemical investigations with MD simulations of the hydrogen-terminated active-site fragment, $^-S-CXYC-SH$, and a full wild-type (*wt*) Trx as well as a P34G Trx mutant in water. Interestingly, the combined results of these MD simulations and the DFT computations on reaction 2 lead to the new insight that the activity of the thioredoxin active-site motif (CXYC) is determined by the structural rigidity associated not only with the particular variable residues (XY) but also with the number of amide N–H groups. The latter are involved in the stabilization of the Cys-32 thiolate. In this way, they determine the acidity and nucleophilicity of this residue.

2. Methods

DFT Calculations. All density functional calculations^{17–19} were carried out with the Amsterdam Density Functional (ADF) program^{20–23} and the QUantum-regions Interconnected by Local Descriptions (QUILD) program.^{25,26} The QUILD program is a wrapper around ADF (and other programs) and is used for its superior geometry optimizer which is based on adapted delocalized coordinates.

Geometries and energies of stationary points occurring in model reaction 1 (i.e., species **1**) were computed at BP86/TZ2P and at OPBE/TZ2P, i.e., with the BP86^{27,28} and OPBE^{29–31} functionals in combination with the TZ2P basis set. The latter is a large uncontracted set of Slater-type orbitals (STOs) containing diffuse functions which is of triple- ζ quality and has been augmented with two sets of polarization functions: 2p and 3d on H, 3d and 4f on C, N, O and S. The core shells of carbon (1s), nitrogen (1s), oxygen (1s) and sulfur (1s2s2p) were treated by the frozen-core approximation.²⁰ An auxiliary set of s, p, d, f and g STOs (fit functions) was used to fit the molecular density and to represent the Coulomb and exchange potentials accurately in each SCF cycle.²⁰

Geometries of stationary points occurring in model reactions 2 and 3 (i.e., species **2** and **3**) were optimized (using analytical gradient techniques) at BP86/TZ2P, except for transition states which were optimized at BP86/DZP. The DZP basis is an uncontracted set of Slater-type orbitals (STOs) of double- ζ quality and has been augmented with one set of polarization functions: 2p on H, 3d on C, N, O, and S.

Energies of stationary points occurring in model reactions 2 and 3 (i.e., species **2** and **3**) were computed at OPBE/TZ2P in a single-point fashion using the BP86/TZ2P (or BP86/DZP) geometries.

All structures were verified by vibrational analyses to be equilibrium geometries (zero imaginary frequencies) or transition states (one imaginary frequency). The character of the normal mode associated with the imaginary frequency of a transition state (i.e., the transition vector) was analyzed to ensure that the correct transition state was found.

Solvent effects in water have been estimated using the Conductor-like Screening Model (COSMO),^{32,33} as implemented in the ADF program.³⁴ We used a solvent-excluding surface with an effective radius for water of 1.9 Å, derived from the macroscopic density and molecular mass, and a relative dielectric constant of 78.4. The radii of the atoms were taken to be MM3 radii,³⁵ divided by 1.2, giving 1.350 Å for H, 1.700 Å for C, 1.608 Å for N, 1.517 Å for O, and 1.792 Å for S.

TABLE 1: Relative Energies (in kcal/mol) of Stationary Points along the Reaction of $CH_3SSCH_3 + CH_3S^-$ (Eq 1), in the Gas Phase and in Water^a

species	in vacuum ^b		in water ^{b,c}	
	OPBE	BP86	OPBE	BP86
$CH_3SSCH_3 + CH_3S^-$	0.00	0.00	0.00	0.00
1RC-1	−8.43	−11.68	−0.70	−0.60
1RC-2	−10.16	−13.09	−1.03	−0.83
1RC-3	—	—	−1.26	−1.08
1TS	−6.31	−9.47	9.06	2.65
1TC	−11.40	−17.05	—	—

^a For structures, see Figures 1 and 2. ^b Computed at OPBE/TZ2P or BP86/TZ2P. ^c Water is simulated with COSMO.

These settings for COSMO comprise an “ab initio” approach to including solvent effects in the QM calculations.³⁶

Molecular Dynamics Simulations. For the simulation of the wild type (*wt*) Trx, we started from a Trx geometry that was previously optimized (starting from an NMR structure with PDB code 1xob) using the ONIOM approach with B3LYP/6-31G(d) for the CGPC active-site moiety, the AMBER Parm94 force field for the rest of the protein, and the TIP3P model for the ca. 5000 discrete water molecules.⁴ The Trx P34G mutant was obtained by subsequent substitution of proline 34 by a glycine.

The starting geometry of the hydrogen-terminated active-site fragment $^-S-CGPC-SH$ system was taken from our BP86/TZ2P optimizations and further processed using the Xleap module of the AMBER 8 package.²⁴ The atomic charges employed were the multipole derived charges (MDC-q)³⁷ from our OPBE/TZ2P calculations, which were used because within AMBER there are no standard charges available for amino-acid residues that are terminated with hydrogen at the C_α position.

Energy minimizations and molecular dynamics simulations were carried out using the SANDER module of the AMBER 8 package²⁴ in the gas phase and in explicit solvent. In the gas phase, the structures were first minimized and then subjected to a molecular dynamics simulation at 300K using Langevin dynamics with a cutoff of 10 Å. The time step was set to 1 fs and the trajectories were saved every 100 steps. The total simulation time was 1 ns.

In explicit solvent, 5 Na^+ counterions were added to neutralize the *wt* Trx and P34G-Trx systems and 1 Na^+ counterion for the CGGC and CGPC systems; then the structures were minimized with explicit solvent (TIP3P box with around 5000 water molecules) using the Parm99 parameter set.³⁸

The MD simulations with solvent were performed using periodic boundary conditions. The system was initially equilibrated at 300 K for 20 ps using Langevin dynamics.³⁹ Production simulations were carried out at 300 K using Langevin dynamics with a collision frequency of 1.0 ps^{−1}. Constant-pressure periodic boundary conditions were used with an average pressure of 1 atm. Isotropic position scaling was used to maintain the pressure with a relaxation time of 2 ps. The time step was set to 2 fs. Shake constraints were applied to all bonds involving hydrogen atoms. The particle mesh Ewald (PME) method was used to calculate electrostatic interactions.⁴⁰ All the intermolecular interactions were treated with a cutoff distance of 10 Å. The trajectories were saved every 100 steps for analysis.

In the smaller $^-S-CGPC-SH$ system, rotation of the dihedrals of the terminal residues is almost free due to the absence of the constraints imposed by the protein structure in full Trx. However, if the substrate were present (which is

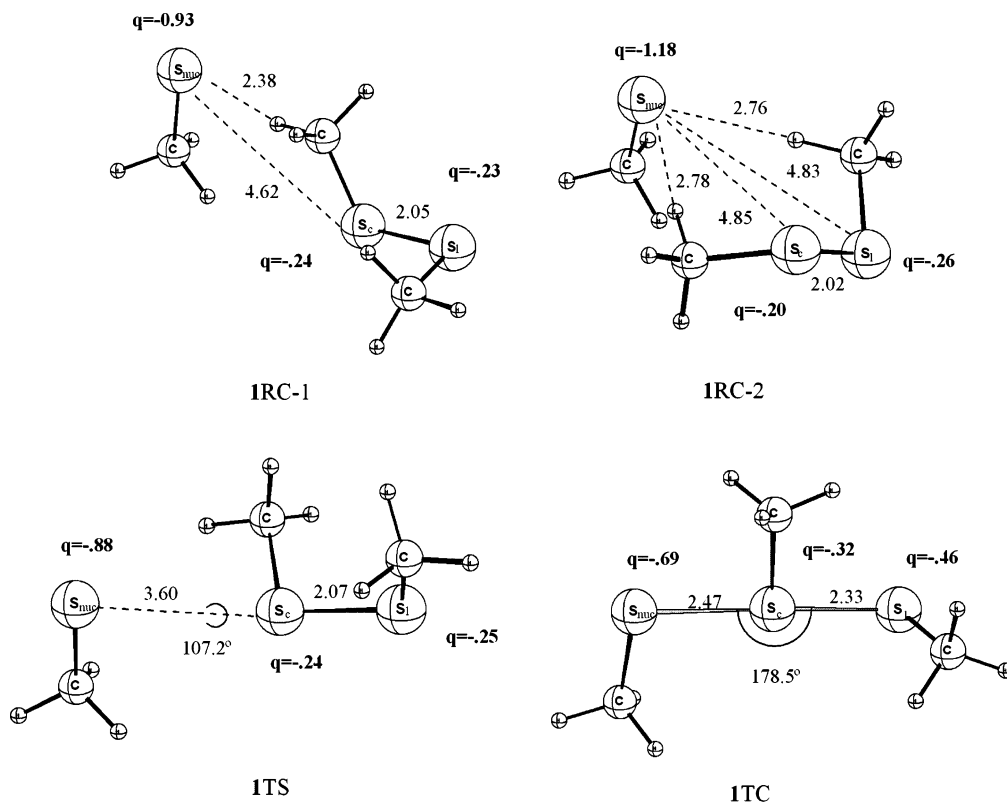


Figure 1. Structures (in Å) and sulfur atomic charges q (in au) for selected species occurring in the model reactions of $\text{CH}_3\text{S}^- + \text{CH}_3\text{SSCH}_3$ (see eq 1) in the gas phase, computed at OPBE/TZ2P (1RC-1, 1RC-2 = reactant complexes; ITS = transition state from 1RC-1 to 1TC; 1TC = transition complex constituted by a hypervalent trisulfide; all structures are singly negatively charged).

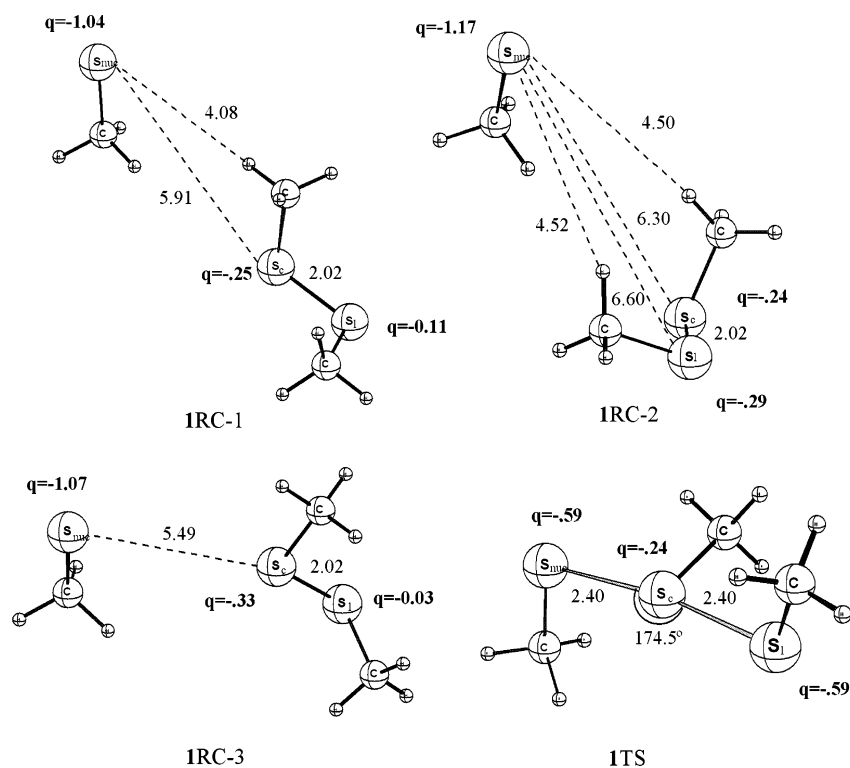


Figure 2. Structures (in Å) and sulfur atomic charges q (in au) for selected species occurring in the model reactions of $\text{CH}_3\text{S}^- + \text{CH}_3\text{SSCH}_3$ (see eq 1) in water, computed with COSMO at OPBE/TZ2P (1RC-1, 1RC-2, 1RC-3 = reactant complexes; ITS = transition state from 1RC-1 to 1TC; 1TC = transition complex constituted by a hypervalent trisulfide; all structures are singly negatively charged).

the situation of interest), the interaction with the thiolate would prevent the rotation of the above-mentioned dihedrals. We have simulated this by fixing the carbons involved in these rotations.

3. Results and Discussion

In the following, we first discuss our DFT results for the archetypal thiol–disulfide exchange of $\text{CH}_3\text{S}^- + \text{CH}_3\text{SSCH}_3$

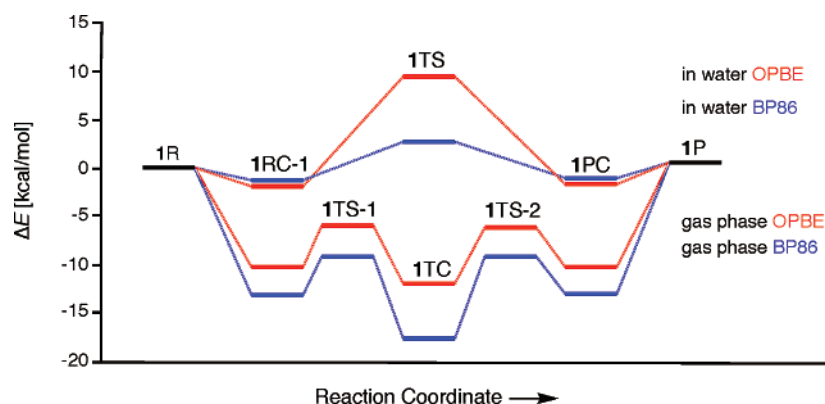


Figure 3. Reaction profile along the $\text{CH}_3\text{S}^- + \text{CH}_3\text{SSCH}_3$ thiol-disulfide exchange ($\text{S}_\text{N}2@\text{S}$) reaction in the gas phase and in water, computed at BP86/TZ2P and OPBE/TZ2P (see Table 1).

(eq 1). Thereafter, we examine the DFT results for our exploration of the thioredoxin-catalyzed disulfide mechanism of the model reaction system $\text{HS-CGPC-S}^- + \text{CH}_3\text{S-SCH}_3$ (eqs 2 and 3). Finally, we consider the MD simulations of *wt* Trx, the P34G mutant thereof as well as the active-site fragment HS-CGPC-S^- .

Thiol-Disulfide Exchange of $\text{CH}_3\text{S}^- + \text{CH}_3\text{SSCH}_3$ in the Gas Phase. The results of our DFT computations on the thiol-disulfide exchange of $\text{CH}_3\text{S}^- + \text{CH}_3\text{SSCH}_3$ (eq 1) are summarized in Table 1 and Figures 1–3. Geometries of selected stationary points, optimized at OPBE/TZ2P are provided in Figures 1 (gas phase) and 2 (aqueous solution); for the corresponding BP86/TZ2P structures, see Figures S1 and S2 in the Supporting Information. Table 1 contains the energies of stationary points relative to reactants, both in the gas phase and in aqueous solution, obtained at OPBE/TZ2P and BP86/TZ2P. These data are visualized as reaction profiles in Figure 3.

We begin with the reaction of $\text{CH}_3\text{S}^- + \text{CH}_3\text{SSCH}_3$ (eq 1). In a recent study on the performance of DFT functionals for describing various $\text{S}_\text{N}2$ reactions, the OPBE functional was found to yield reaction profiles, in particular, activation energies, in good agreement with high-level *ab initio* CCSD(T) benchmarks.^{14,15} The BP86 functional, on the other hand, is known to perform better for describing hydrogen-bond distances and energies, but it seriously underestimates reaction barriers.^{41,42} In the present case, we see that geometries obtained with either OPBE/TZ2P or BP86/TZ2P are in good agreement (compare Figures 1 and 2 with Figures S1 and S2). Covalent bonds (e.g., S–S distances) agree within a few hundredths of an angstrom. The weak intermolecular $\text{S}^-\cdots\text{H-C}$ hydrogen bonds show larger differences between OPBE/TZ2P and BP86/TZ2P, that is, by a few tenths of an angstrom up to about 1 Å but this is less relevant in the sense that in either DFT approach such variations in the length of these weak bonds correspond to only small changes in the energy (about a kcal/mol or less).

As can furthermore be seen in Table 1 and Figure 3, OPBE/TZ2P and BP86/TZ2P yield qualitatively similar reaction profiles. But indeed BP86 overestimates the stability of the hypervalent transition species by about 6 kcal/mol as compared to OPBE/TZ2P, both in the gas phase and in water. On the other hand, we found that BP86/TZ2P optimizations are numerically more robust and are computationally more efficient in finding equilibrium structures of the weakly bound reactant and product complexes than OPBE/TZ2P optimizations. This may be ascribed to the fact that BP86 optimizations are associated with somewhat less shallow potential wells than the latter method.

Thus, the larger and computationally more demanding model reactions of eqs 2 and 3 have been carried out in a hybrid

TABLE 2: Relative Energies (in kcal/mol) of Stationary Points along the Reaction of $\text{CH}_3\text{SSCH}_3 + \text{CGPC}$ (Eqs 2 and 3), in the Gas Phase and in Water^a

species	in vacuum ^b		in water ^{b,c}	
	OPBE	BP86	OPBE	BP86
$\text{CH}_3\text{SSCH}_3 + \text{CGPC}$	0.00	0.00	0.00	0.00
Step 1 (eq 2)				
2RC-1	−1.16	−2.43	2.89	−0.50
2RC-2	−1.54	−5.06	3.23	−0.85
2RC-3			3.78	−0.64
2TS-1	2.22 ^d	−2.12 ^d	14.96 ^d	12.11 ^d
2TS-2	25.31 ^d	22.86 ^d		
2TC-1	0.79	−2.82		
2TC-2	7.12	−3.15		
2PC-1	4.69	−1.49	6.83	3.11
2PC-2	3.70	2.80	2.80	0.87
2PC-3	9.57	6.96	0.84	1.24
Step 2 (eq 3)				
3RC-1 + CH_3SH	4.87	7.77	1.23	1.26
3RC-2 + CH_3SH			3.34	0.60
3TS-1 + CH_3SH	12.41 ^d	10.58 ^d	29.46 ^d	22.90 ^d
3TC + CH_3SH	8.43	4.22		
3TS-2 + CH_3SH	30.99 ^d	29.42 ^d		
3PC + CH_3SH	27.12	24.93	9.03	14.00
3P + $\text{CH}_3\text{SH} + \text{CH}_3\text{S}^-$	40.32	44.96	2.16	9.73

^a See Figures 4 and 5 for structures. ^b Computed at OPBE/TZ2P//BP86/TZ2P or BP86/TZ2P, unless stated otherwise. ^c Water is simulated with COSMO. ^d Computed at OPBE/TZ2P//BP86/DZP or BP86/TZ2P//BP86/DZP.

approach based on BP86 geometries in combination with the more accurate OPBE/TZ2P energies obtained in a single-point manner. However, in the remainder of this section, we discuss the OPBE/TZ2P results for the reaction of $\text{CH}_3\text{S}^- + \text{CH}_3\text{SSCH}_3$ (eq 1).

In the gas phase, the $\text{S}_\text{N}2@\text{S}$ reaction of $\text{CH}_3\text{S}^- + \text{CH}_3\text{SSCH}_3$ proceeds via a symmetric triple-well PES which involves a central transition complex (1TC) separated by a pre- and post-transition state (both correspond to 1TS) from reactant and product complexes, respectively (both correspond to 1RC-1; see Figures 1 and 3). In 1RC-1, CH_3S^- enters into a hydrogen-bonding interaction of −8.4 kcal/mol with a methyl C–H bond on one side of CH_3SSCH_3 ($\text{S-H} = 2.4$ Å; see Table 1 and Figure 1). There is also an alternative reactant or product complex 1RC-2 in which a symmetric (bifurcated) hydrogen bond is formed between CH_3S^- and a C–H bond on each of the two methyl groups ($\text{S-H} = 2.8$ Å); this species is slightly more stable ($\Delta E = -10.2$ kcal/mol). From 1RC-1 at −8.4 kcal/mol, the reaction proceeds via transition state 1TS at −6.3 kcal/mol to the stable trisulfide 1TC at −11.4 kcal/mol (see Table 1). Similar reaction profiles were found by Bachrach and Mulhearn for the symmetric thiol-disulfide exchange reaction of $\text{SH}^- + \text{CH}_3\text{SSH}$.^{8,9}

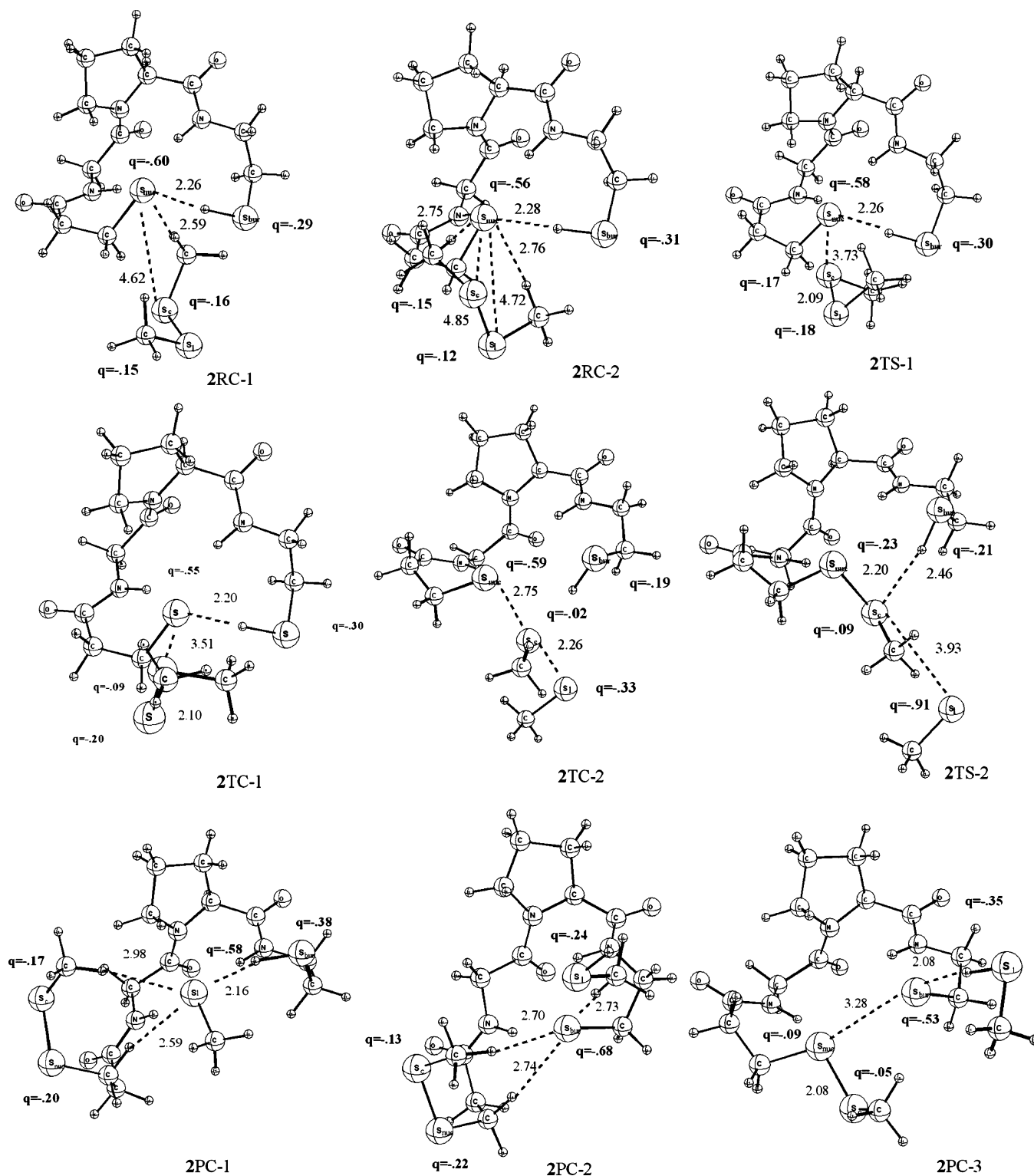


Figure 4. Structures (in Å) and sulfur atomic charges q (in au) for selected species occurring in the model reactions of $\text{HS-CGPC-S}^- + \text{CH}_3\text{S-SCH}_3$ (see eq 2; step 1 of Scheme 2) in the gas phase, computed at BP86 (2RC-1, 2RC-2 = reactant complexes; 2TC = transition complex constituted by a hypervalent trisulfide; 2TS-1, 2TS-2 = transition states; 2PC-1, 2PC-2, 3PC-3 = product complexes; all structures are singly negatively charged).

Thiol–Disulfide Exchange of $\text{CH}_3\text{S}^- + \text{CH}_3\text{SSCH}_3$ in Water. Going from the gas phase to aqueous solution, the triple-well PES turns essentially into a unimodal reaction profile which proceeds from the reactants directly to the trisulfide which is now a transition state (ITS) at +9.1 kcal/mol at COSMO-OPBE/TZ2P (see Table 1). Note that the reactant and product complexes do not disappear completely but they are only very

little pronounced on the PES with a complexation energy of only -0.7 or -1.0 kcal/mol for 1RC-1 and 1RC-2, respectively (see Table 1). The S–S bond distances in 1TS amount to 2.4 Å (see Figure 2). Our findings agree nicely with earlier work of Hayes and Bachrach on archetypal $\text{S}_2\text{@S}$ reactions in solution.^{8b} The disappearance of the characteristic triple-well structure on the PES of this $\text{S}_2\text{@S}$ reaction and the transfor-

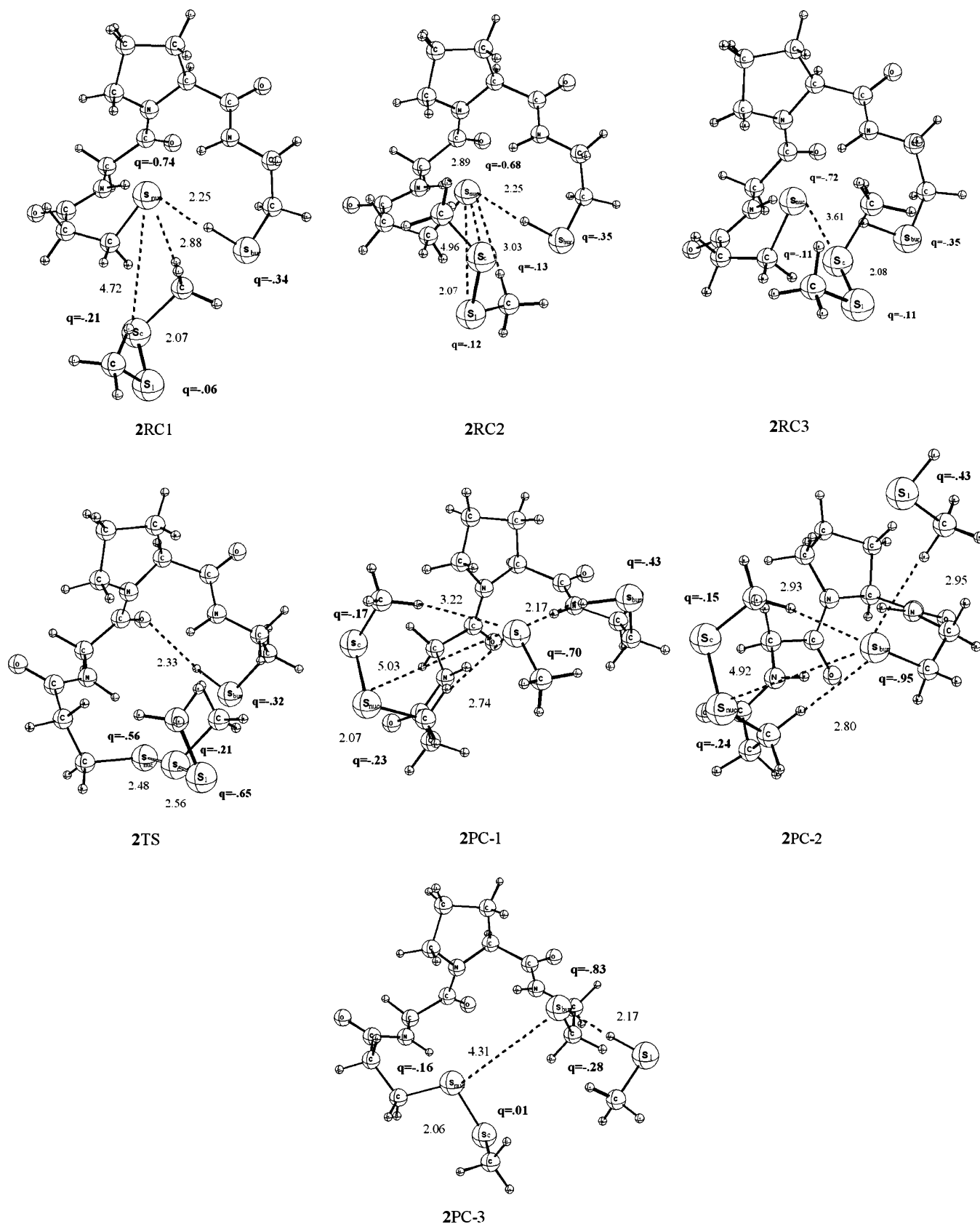


Figure 5. Structures (in Å) and sulfur atomic charges q (in au) for selected species occurring in the model reactions of $\text{HS-CGPC-S}^- + \text{CH}_3\text{S-SCH}_3$ (see eq 2; step 1 of Scheme 2) in water, computed with COSMO at BP86 (2RC-1, 2RC-2, 2RC-3 = reactant complexes; 2TS = transition state constituted by a hypervalent trisulfide; 2PC-2, 2PC-3 = product complexes; 2PC-1 = intermediate; all structures are singly negatively charged).

mation into a unimodal reaction profile in solution is also in line with similar findings for anionic $\text{S}_{\text{N}}2@Si$ and $\text{S}_{\text{N}}2@P$ reactions.⁴³

Catalytic Disulfide Reduction: Mixed Disulfide Formation in the Gas Phase. Next, we consider the reduction of dimethyl disulfide by the hydrogen terminated active-site fragment of

thioredoxin. As mentioned above, our DFT computations on this problem have been done at OPBE/TZ2P//BP86. We begin with the first step of the reaction of $\text{HS-CGPC-S}^- + \text{CH}_3\text{S-SCH}_3$, i.e., the mixed disulfide formation (eq 2). The results are summarized in Table 2 and Figures 4 and 5.

The gas-phase reaction profile of step 1 of the reaction mechanism, that is, the thiol–disulfide exchange of $\text{HS-CGPC-S}^- + \text{CH}_3\text{S-SCH}_3$ (eq 2), is again a triple-well PES, similar to that for the smaller model reaction of eq 1. Thus, we find structurally similar reactant complexes (2RC-1 and 2RC-2; see Figure 4) which are, however, significantly more weakly bound than those smaller model system, with complexation energies of less than -2 kcal/mol (see Table 2). This small interaction energy is clearly not sufficient to account for the binding of the substrate to the full Trx protein under physiological conditions. In the latter, the hydrophobic patch of residues at the surface near the active site must therefore have an additional stabilizing effect for the binding of the substrate to Trx to occur.

The transition species is again a stable trisulfide (2TC-1) at $+0.8$ kcal/mol, separated from reactant and product complexes by a pre-transition state (2TS-1) at 2.2 kcal/mol and a high-energy post-transition state (2TS-2) at 25.3 kcal/mol, respectively (see Table 2). Note that the S–S bonds in the trisulfide moiety of 2TC-1 are pronouncedly asymmetric: the $\text{S}_{\text{nuc}}\text{--S}_{\text{c}}$ bond distance is long, 2.75 Å, and the $\text{S}_{\text{c}}\text{--S}_{\text{l}}$ bond distance is short, 2.26 Å (see Figure 4).

Interestingly, the longer $\text{S}_{\text{nuc}}\text{--S}_{\text{c}}$ distance in 2TC-1 appears to be due to hydrogen bonding of the partially negatively charge $\text{S}_{\text{nuc}}^{\delta-}$ with amide N–H groups as well as the thiol group of the buried Cys-35 (see Figure 4). The Gly-Pro amide bond cannot contribute to such stabilizing interactions with the nucleophilic thiolate because it does not involve N–H bonds. The stabilizing effect of the $\text{S}_{\text{nuc}}^{\delta-}\cdots\text{H}\text{--S}_{\text{bur}}$ hydrogen bond in 2TC-1 is also illustrated by the fact that the related trisulfide 2TC-2, in which we have broken this contact, is about 6 kcal/mol higher in energy than 2TC-1 (see Table 2 and Figure 4). Thus, the stabilization of the thiolate associated with these hydrogen bonds makes the Cys-32 thiolate effectively less nucleophilic. Note that these hydrogen bonds also make the Cys-32 thiol group more acidic which facilitates its deprotonation in solution.

The relatively high energy of 25.3 kcal/mol of the post-transition state 2TS-2 originates from the fact that the evolving CH_3S^- leaving group receives initially no stabilizing interactions but the attacking nucleophile (the Cys-32 thiolate) does, namely, by the amide N–H groups (see Figure 4). Eventually, however, the CH_3S^- leaving group reaches the thiol group of the buried Cys-35 and enters into a stabilizing $\text{CH}_3\text{S}^-\cdots\text{H}\text{--S}_{\text{bur}}$ hydrogen bond in the product complex 2PC-1 at 4.7 kcal/mol (see Table 2 and Figure 4).

Strikingly, product complex 2PC-1 at 4.6 kcal/mol can rearrange easily into other product complex structures, such as 2PC-3 at 9.6 kcal/mol or 2PC-2 at 3.7 kcal/mol, in which the proton of the buried thiol group has been abstracted by the leaving group (see Table 2 and Figure 4). We recall the controversy regarding the mechanism of deprotonation of the buried cysteine as required to activate the second $\text{S}_{\text{N}}2@S$ step that leads to product formation (eq 3). Previously, it was hypothesized⁷ that this deprotonation is carried out by the conserved aspartate residue Asp-26 at more than 6 Å from the buried Cys-35, possibly with the help of a water molecule.

Our data suggest a new and straightforward mechanism for the deprotonation of the buried cysteine, namely, that it occurs

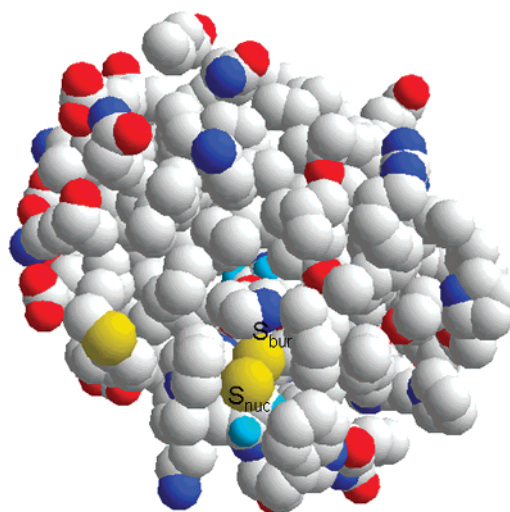


Figure 6. Van der Waals representation of thioredoxin from an ONIOM geometry optimization in ref 5. S_{nuc} is the thiolate sulfur atom of the nucleophilic cysteine, and S_{bur} is the sulfur in the thiol of the buried cysteine.

directly after the first $\text{S}_{\text{N}}2@S$ step through proton abstraction by the leaving group which is released in the vicinity of the thiol group of the buried Cys-35. In solution, we estimate the barrier height of this facile proton transfer to be ca. 1 kcal/mol (see below).

Our findings regarding the mechanism of Trx-catalyzed disulfide reduction also shed light on the controversy regarding the different experimental pK_{a} values measured for the nucleophilic and buried cysteines (Cys-32 and Cys-35). The Trx structure in Figure 6 shows that the buried Cys-35 is initially protected by the nucleophilic Cys-32.⁵ The latter has a lower pK_{a} due to the stabilizing hydrogen bonds with amide N–H groups and due to the microdipoles and shielding of the α helix, and the buried Cys-35 has a $\text{pK}_{\text{a}} > 12$.⁵ The displacement of the nucleophilic Cys-32 as promoted by the binding of the substrate should make the buried cysteine accessible for the substrate and solvent. Thus, in the mixed disulfide, the buried Cys-35 is much less shielded and its pK_{a} decreases to the value of a normal cysteine, i.e., around 8.5, and has also become accessible to the methylthiolate leaving group, which abstracts a proton.

Catalytic Disulfide Reduction: Mixed Disulfide Formation in Water. Similar to the situation for eq 1, going from the gas phase to aqueous solution, the triple-well PES of eq 2 turns essentially into a unimodal reaction profile which proceeds from the reactants directly to the trisulfide which becomes a transition state (2TS-1) at +15 kcal/mol at COSMO-OPBE/TZ2P//BP86 (see Table 2). The reactant and product complexes do again not disappear completely from the PES (see also the BP86 energies for these species) but they are only very little pronounced on the PES (see Table 2).

The transition vector of 2TS-1 corresponds to $\text{S}_{\text{nuc}}\text{--S}_{\text{c}}$ bond formation between enzyme and substrate and the breaking of the bond between the S_{c} and S_{l} of the leaving group. The two S–S bonds in the trisulfide 2TS-1 adopt again different lengths, i.e., $\text{S}_{\text{nuc}}\text{--S}_{\text{c}} = 2.48$ Å and $\text{S}_{\text{c}}\text{--S}_{\text{l}} = 2.56$ Å (see Figure 5) but the differences are significantly smaller than for 2TC-1 in the gas phase (compare Figure 4). Note also that the relative S–S lengths have inverted: in the gas phase, the nucleophile is further from S_{c} than the leaving group whereas here, in water, the leaving group is in a more advanced stage of departure due to

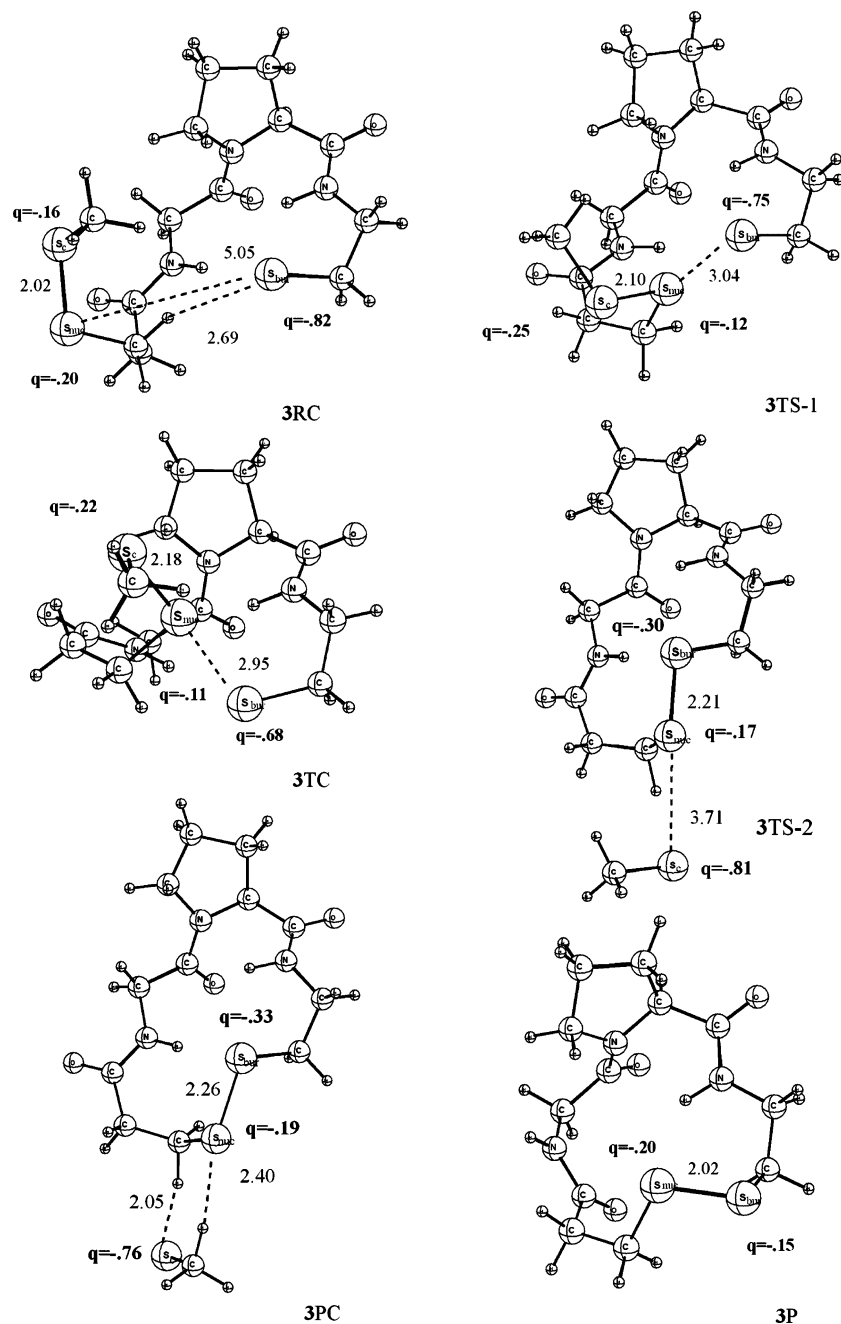


Figure 7. Structures (in Å) and sulfur atomic charges q (in au) for selected species occurring in the model reactions of ${}^-\text{S}-\text{CGPC}-\text{S}-\text{SCH}_3$ (see eq 3; step 2 of Scheme 2) in the gas phase, computed at BP86 (3RC = reactant complex; 3TS-1, 3TS-2 = transition states; 3TC = transition complex constituted by a hypervalent trisulfide; 3PC = product complex; 3P = product; all structures are singly negatively charged).

the stabilizing effect of solvation. This, in turn, enables the nucleophile to approach somewhat more closely (compare 2TC-1 and 2TS-1 in Figures 4 and 5, respectively).

Importantly, also our data for aqueous solution suggest the new mechanism for the deprotonation of the buried Cys-35, that is, proton abstraction by the leaving group, directly after the first $\text{S}_\text{N}2@\text{S}$ step. Thus, we find that in the product complex 2PC-1, at 6.8 kcal/mol relative to reactants (see Table 2), the thiolate leaving group establishes $\text{S}_\text{L}^- \cdots \text{H}-\text{S}_\text{bur}$ hydrogen bonds with the thiol group of the buried Cys-35, besides forming the energetically less important hydrogen bonds with the methyl C-H bonds of the mixed disulfide (see Figure 5). Product complex 2PC-1 at 6.8 kcal/mol can rearrange easily into other product complex structures, such as the more stable 2PC-2 at 2.8 kcal/mol, in which the proton of the buried thiol group has been abstracted by the leaving group (see Table 2 and Figure

5). The barrier height of this facile proton transfer is estimated to be 0.5 kcal/mol at COSMO-OPBE//BP86 and 1.3 kcal/mol at COSMO-BP86 using the simple model reaction $\text{CH}_3\text{S}^- + \text{HSCH}_3 \rightarrow \text{CH}_3\text{SH} + {}^-\text{SCH}_3$ and the TZ2P basis for all species. As indicated before, this new and straightforward mechanism is inherently competitive with the earlier hypothesized mechanism⁷ of a possibly solvent-mediated deprotonation by the conserved aspartate residue Asp-26 at more than 6 Å from the buried Cys-35.

Catalytic Disulfide Reduction: Product Formation in the Gas Phase. We now arrive at the second and final step of the reduction of dimethyl disulfide by the hydrogen terminated active-site fragment of thioredoxin, that is, product formation as shown in eq 3 through intramolecular thiol–disulfide exchange of the activated (i.e., deprotonated Cys-35) mixed disulfide ${}^-\text{S}-\text{CGPC}-\text{S}-\text{SCH}_3$ that results after step 1 (see also

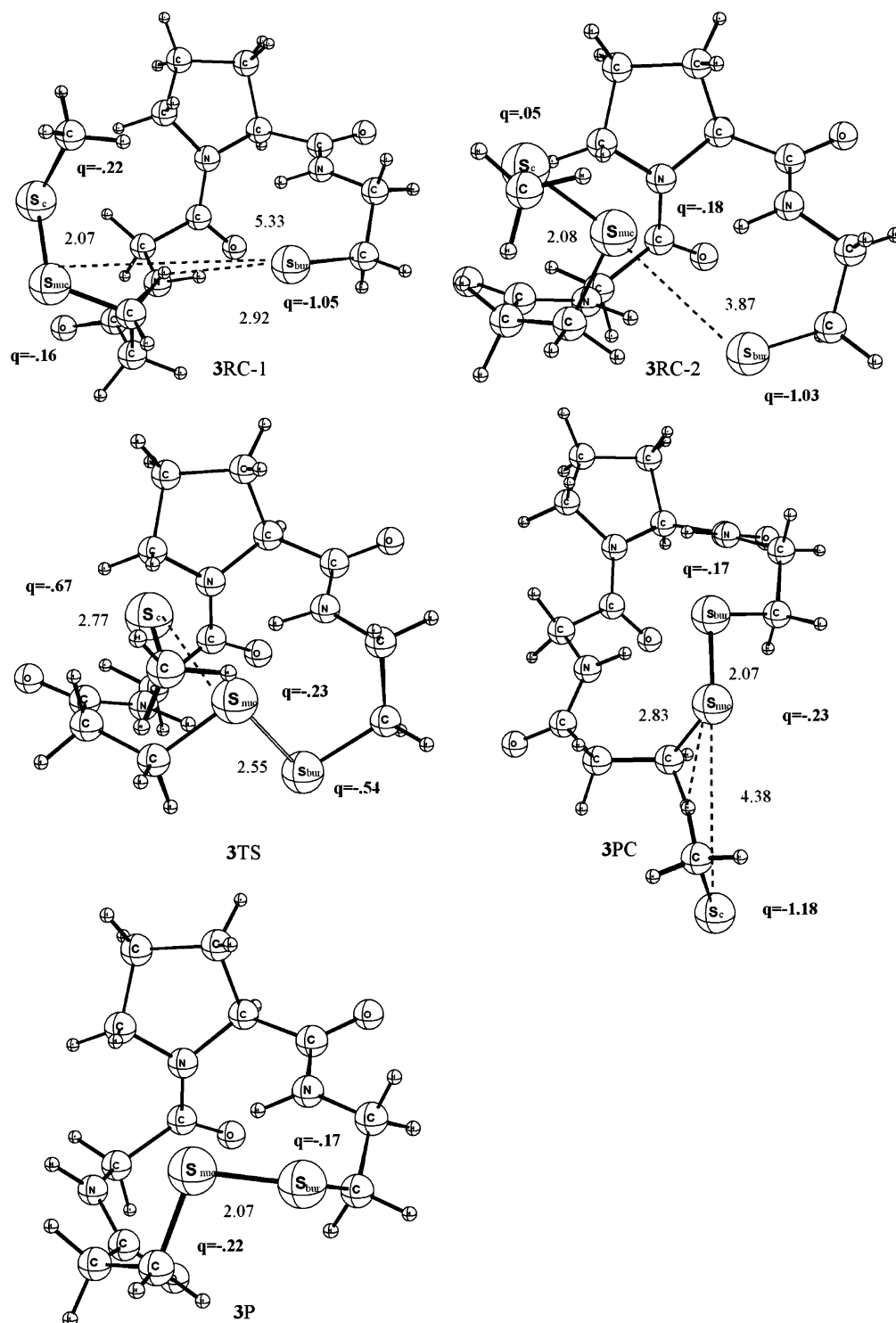


Figure 8. Structures (in Å) and sulfur atomic charges q (in au) for selected species occurring in the model reactions of $^-S-CGPC-S-SCH_3$ (see eq 3; step 2 of Scheme 2) in water, computed with COSMO at BP86 (3RC-1, 3RC-2 = reactant complexes; 3TS = transition state constituted by a hypervalent trisulfide; 3PC = product complex; 3P = product; all structures are singly negatively charged).

Scheme 2 for an overview). We recall that our DFT computations on this problem have been done at OPBE/TZ2P//BP86. The results are summarized in Table 2 and Figures 7 and 8.

Complete departure of the protonated leaving group from the activated mixed disulfide $CH_3SH \cdots ^-S-CGPC-S-SCH_3$ (2PC-2 at 3.7 kcal/mol) that is formed in the first step leads to $^-S-CGPC-S-SCH_3$ (3RC-2 at 4.9 kcal/mol relative to the original reactants; see Table 2). From here, the thiol–disulfide exchange reaction proceeds again via a triple-well mechanism that is characteristic for slightly sterically hindered $S_N2@S$

reactions in the gas phase, similar to the mechanism discussed in detail above for the mixed-disulfide formation. Thus, we go from 3RC-2 at 4.9 kcal/mol via a pre-transition state 3TS-1 at 12.4 kcal/mol to a stable trisulfide transition complex 3TC at 8.4 kcal/mol (see Table 2). Transition complex 3TC has somewhat asymmetric $S_{bur}-S_{nuc}$ and $S_{nuc}-S_c$ bond distances of 2.95 and 2.18 Å, respectively (see Figure 7). Thereafter, we go via a high-energy post-transition state 3TS-2 at 31.0 kcal/mol to the product complex $CH_3S \cdots ^-S-CGPC-S$, i.e., 3PC

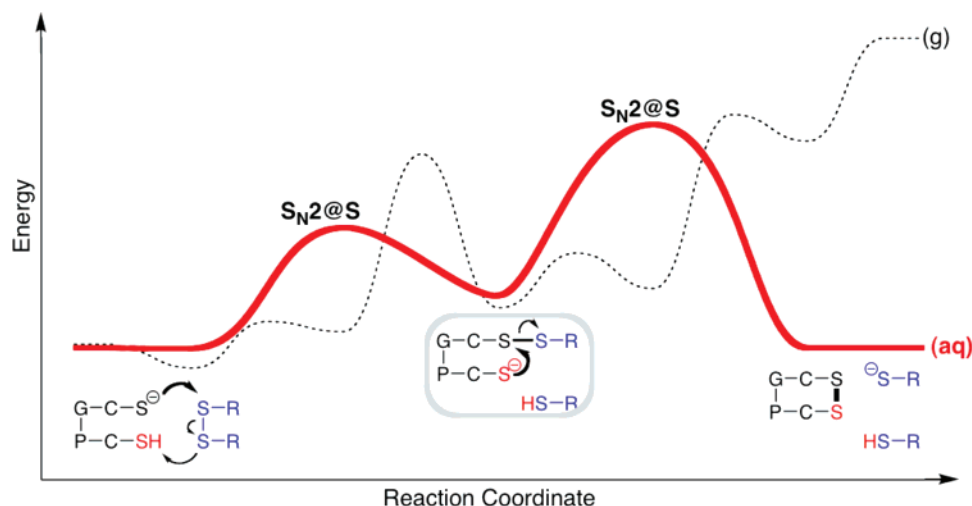


Figure 9. Schematic reaction profile for CGPC-catalyzed reduction of dimethyl disulfide along the successive reactions 2 and 3 in the gas phase (dashed curve) and in water (red curve), emerging from our computations (see also text and Table 2). Note that the leaving group of the first $S_N2@S$ step deprotonates and thus activates the buried thiol group (in red) for the second $S_N2@S$ step.

at 27.1 kcal/mol, which eventually dissociates into product and oxidized enzyme **3P** at 40.3 kcal/mol (see Table 2 and Figure 7). Note that product formation (eq 3) in the gas phase is overall more than 35 kcal/mol endothermic.

Catalytic Disulfide Reduction: Product Formation in Water. Similar to the situation for eqs 1 and 2, going from the gas phase to aqueous solution, the triple-well PES of eq 3 turns essentially into a unimodal reaction profile which proceeds from the reactants directly to the trisulfide which becomes a transition state (**3TS-1**) at +29 kcal/mol relative to the original reactants at COSMO-OPBE/TZ2P//BP86 (see Table 2). Note that this corresponds to a reaction barrier of ca. 28 kcal/mol for this product forming reaction step (see Table 2). The S_c-S_{nuc} and $S_{nuc}-S_{bur}$ bond distances in **3TS-1** amount to 2.77 and 2.55 Å, respectively; i.e., the leaving group is in an advanced stage of departure (see Figure 8).

The product complexes do again not disappear from the PES but they are no longer more stable than the final product (see Table 2). The product complexes occur in many conformers which we have not all resolved. These conformers (e.g., **3PC** at 9 kcal/mol) can interconvert or proceed to the products, i.e., the reduced substrate $CH_3S^- (+CH_3SH)$ + the oxidized enzyme $S-CGPC-S$ (**3P** at 2 kcal/mol), via low-barrier isomerization reactions (see Table 2 and Figure 7; see also the BP86 energies for these species).

In Figure 9, we have summarized the PES data in the form of an overall reaction profile. The bold red curve corresponds to the reaction mechanism in aqueous solution. Note that the low-barrier deprotonation of the buried Cys-35 after $S_N2@S$ step 1 is not explicitly shown in Figure 9. For comparison, the more complex gas-phase reaction profile (composed of two triple-well $S_N2@S$ reactions) is also depicted in Figure 9 as a black dotted curve. Thus, we can see that the overall Trx-catalyzed dimethyl disulfide model reaction in aqueous solution is, with a reaction energy of +2 kcal/mol, nearly thermoneutral (see Table 2). Also each of the two $S_N2@S$ steps are only slightly endothermic or close to thermoneutral. They are associated with a reaction barrier of some 15 kcal/mol in the first step (eq 2) and 28 kcal/mol in the second step (eq 3). The second step (eq 3) is thus rate determining.

Molecular Dynamics Analysis. As mentioned before, the presence of the backbone amide groups, which engage in hydrogen bonding with the thiolate, stabilizes the reagents (S^-)

in relation to the intermediates (S^δ^-), turning it into a less effective nucleophile and making the reaction less favorable. The CGPC system, which is equal to the motif in the enzyme, has a $S_{nuc}-S_c$ bond weaker than the S_c-S_l bond, as can be observed by the bond distances in the structure of the trisulfide anion (see Figures 4, 5, 7, and 8).

Does this mean that the smaller systems are not good models because the lack of the remaining of the protein allows the mentioned interactions? Or, in opposition, does the thiolate of the CXYC motif embedded in the remaining of the enzyme engage in the same pattern of H-bonding that is observed in the small systems?

To verify this, we performed MD simulations of the *wt* enzyme and with the proline of the CGPC motif replaced by a glycine and compared it with the smaller system (both in the gas phase and with explicit solvent).

The results are very interesting. In the enzyme with the CGGC motif we have one more potential hydrogen bond donor. However, the protein structure seems to restrain the thiolate to engage in hydrogen bonding mainly with two of the amide groups. In the gas phase we detected hydrogen bonding to the Gly34 and Cys35 NH groups during 99 and 100% of the simulation time, and to Gly33 NH during only 21% of the time. In explicit solvent we detected hydrogen bonding to Gly33 NH during 67% of the simulation time and to Gly34 during 43%; Cys35 NH is too far away to engage in this kind of interaction. The difference in the pattern of hydrogen bonds in the gas phase and explicit solvent is due to the rotation of the side chain of the nucleophilic cysteine in solvent in such a way that the thiolate becomes more exposed.

For the *wt* enzyme in the gas phase, the thiolate can engage in hydrogen bonding with any of the two available NH groups (81% with the Gly33 NH and 100% with the Cys35 NH). In solvent, the thiolate engages in hydrogen bonding with the Gly33 NH during 98% of the simulation time, the Cys35 NH is too far away.

For the CGPC system, we mainly observed hydrogen bonding between the thiolate and Gly NH. In the gas phase, this hydrogen bond is detected during 94% and in solvent during 70% of the simulation time. In both cases the terminal Cys NH is too far away. Consequently, this amide-thiolate interaction occurs not only in the small systems but also in the enzyme. The effect is stronger in the gas phase.

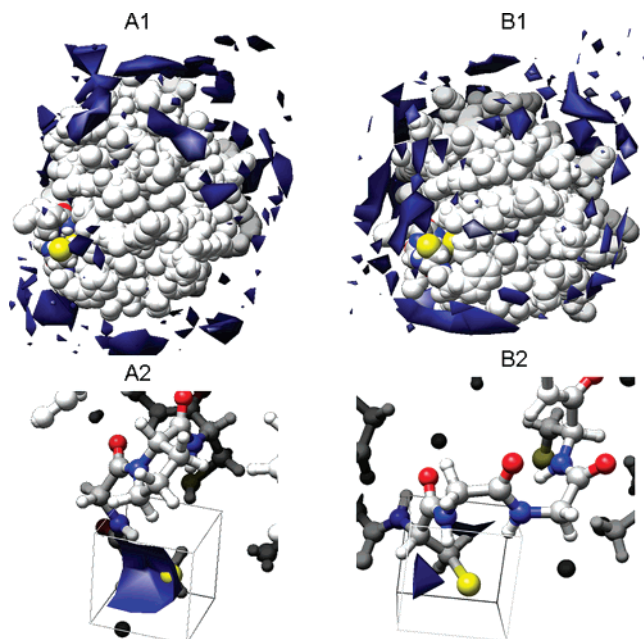


Figure 10. Water density around the *wt* (A1 and A2) and P34G (B1 and B2) enzymes.

We also performed water analysis on the simulations of *wt* and P34G enzymes. We found that, as expected, the thiolate in the CGPC motif is more solvated than in the CGGC motif because it is involved in one less hydrogen bond with the amide groups of the backbone (Figure 10).

The amide group of Cys35 has to be always present because the $S\gamma$ of this residue performs a fundamental role in the second step of the mechanism and so this is a conserved residue. However, the residues between the two cysteines vary among thioredoxin family members. We think that the proline residue in the CXYC motif of thioredoxin might not have a structural role only: in addition, the lack of the NH in this residue could favor the nucleophilic attack of the thiolate. Interestingly, other important members of the thioredoxin family, Glutaredoxins, have prolines in their CXYC motifs (in position Y). Glutaredoxins are also reducing enzymes.

Structurally similar but functionally different enzymes are PDI and DsbA. PDI can play the role of an oxidant or an isomerase, and DsbA is an oxidant. DsbA has also a proline in the CXYC motif. However, it is next to a D-histidine (which has one NH groups in the side chain) and PDI has a glycine and a D-histidine.

4. Conclusions

We have computationally explored the reaction mechanism of the thioredoxin-catalyzed reduction of dimethyl disulfide using both density functional theory and classical molecular dynamics. In aqueous solution, the mechanism involves two distinct $S_N2@S$ reactions, each of which proceeds via a trisulfide transition state: (i) first, the thiolate of the nucleophilic cysteine (Cys-32) attacks the disulfide leading to the formation of the mixed-disulfide intermediate; (ii) second, the thiolate of the deprotonated buried cysteine (Cys-35) attacks the mixed disulfide at the sulfur atom of Cys-32 leading to the formation of the final products of reduction plus the enzyme in its oxidized state.

Interestingly, our data suggest a new and straightforward mechanism for the deprotonation of the buried cysteine, which is required to activate the second $S_N2@S$ step. The current

hypothesis is that this deprotonation occurs through a solvent-mediated proton transfer to the aspartate residue Asp-26 at more than 6 Å from the buried Cys-35. Our DFT computations suggest instead that deprotonation occurs directly after the first $S_N2@S$ step through proton abstraction by the leaving group which is released in the vicinity of (in fact, in steric contact with) the thiol group of the buried Cys-35.

The combined results of our MD simulations and the DFT computations on the first reaction step of thioredoxin-catalyzed disulfide reduction furthermore show that the activity of the thioredoxin active-site motif (CXYC) is determined not only by the structural rigidity associated with the particular variable residues (XY) but also by the number of amide N–H groups. The latter are involved in the stabilization of the Cys-32 thiolate and thus affect the acidity and nucleophilicity of this residue.

Finally, we found that the reaction profile of the archetypal thiol–disulfide exchange reaction of $CH_3S^- + CH_3SSCH_3$ (eq 1) changes from a triple-well PES with a stable trisulfide intermediate in the gas phase to an essentially unimodal PES with a central barrier provided by a trisulfide transition state in the aqueous phase. Similar behavior is also found for the more complex $S_N2@S$ substitutions occurring in the model reaction for thioredoxin-catalyzed disulfide reduction proceeding from $HS-CGPC-S^- + CH_3SSCH_3$ (eqs 2 and 3).

The insights gained in this study may help understand more generally the determinants that are responsible for the diverse functions of the various enzymes in the thioredoxin family.

Acknowledgment. We thank the Fundação para a Ciência e Tecnologia (FCT, Portugal) for financial support and the fellowship SFRH/BD/17845/2004. We also thank The Netherlands Organization for Scientific Research (NWO–CW and NWO–NCF) for financial support.

Supporting Information Available: Geometries, vibrational analyses (number of imaginary frequencies), and total energies of stationary points. This material is available free of charge via the Internet at <http://pubs.acs.org>.

References and Notes

- (1) Carvalho, A. T. P.; Fernandes, P. A.; Ramos, M. J. *Prog. Biophys. Mol. Biol.* **2006**, *91*, 229.
- (2) Berg, J. M.; Tymoczko, J. L.; Stryer, L. *Biochemistry*, 5th ed.; W. H. Freeman and Co.: New York, 2002.
- (3) Holmgren, A. *Structure* **1995**, *3*, 239.
- (4) Carvalho, A. T. P.; Fernandes, P. A.; Ramos, M. J. *J. Phys. Chem. B* **2006**, *110*, 5758.
- (5) Carvalho, A. T. P.; Fernandes, P. A.; Ramos, M. J. *J. Comput. Chem.* **2006**, *27*, 966.
- (6) Chivers, P. T.; Raines, R. T. *Biochemistry* **1997**, *36*, 15810.
- (7) Menchise, V.; Corbier, C.; Didierjean, C.; Saviano, M.; Benedetti, E.; Jacquot, J. P.; Aubry, A. *Biochem. J.* **2001**, *359*, 65.
- (8) (a) Bachrach, S. M.; Mulhearn, D. C. *J. Phys. Chem.* **1996**, *100*, 3535. (b) Hayes, J. M.; Bachrach, S. M. *J. Phys. Chem. A* **2003**, *107*, 7952–7961. (c) Bachrach, S. M.; Chamberlin, A. C. *J. Org. Chem.* **2003**, *68*, 4743.
- (9) (a) Bachrach, S. M.; Walker, C. J.; Lee, F.; Royce, S. *J. Org. Chem.* **2007**, *72*, 5174. (b) Bachrach, S. M.; Woody, J. T.; Mulhearn, D. C. *J. Org. Chem.* **2002**, *67*, 8983.
- (10) Dmitrenko, O.; Thorpe, C.; Bach, R. D. *J. Org. Chem.* **2007**, *72*, 8298.
- (11) (a) Bento, A. P.; Bickelhaupt, F. M. *J. Org. Chem.* **2007**, *72*, 2201. (b) van Bochove, M. A.; Swart, M.; Bickelhaupt, F. M. *J. Am. Chem. Soc.* **2006**, *128*, 10738.
- (12) Gordon, M. S.; Windus, T. L.; Burggraf, L. W.; Davis, L. P. *J. Am. Chem. Soc.* **1990**, *112*, 7167.
- (13) Gonzales, J. M.; Pak, C.; Cox, R. S.; Allen, W. D.; Schaefer, H. F.; Császár, A. G.; Tarczay, G. *Chem. Eur. J.* **2003**, *9*, 2173.
- (14) Swart, M.; Solà, M.; Bickelhaupt, F. M. *J. Comput. Chem.* **2007**, *28*, 1551.

- (15) Bento, A. P.; Solà, M.; Bickelhaupt, F. M. *J. Comput. Chem.* **2005**, *26*, 1497.
- (16) Fernandes, P. A.; Ramos, M. J. *Chem. Eur. J.* **2003**, *9*, 5916.
- (17) Hohenberg, P.; Kohn, W. *Phys. Rev. B* **1964**, *136*, B864.
- (18) Kohn, W.; Sham, L. J. *Phys. Rev.* **1965**, *140*, 1133.
- (19) Parr, R. G.; Yang, W. *Density-Functional Theory of Atoms and Molecules*; Oxford University Press: New York, 1989.
- (20) te Velde, G.; Bickelhaupt, F. M.; Baerends, E. J.; Fonseca Guerra, C.; van Gisbergen, S. J. A.; Snijders, J. G.; Ziegler, T. *J. Comput. Chem.* **2001**, *22*, 931.
- (21) Bickelhaupt, F. M.; Baerends, E. J. In *Reviews in Computational Chemistry*; Lipkowitz, K. B., Boyd, D. B., Eds.; Wiley-VCH: New York, 2000; Vol. 15, pp 1–86.
- (22) Baerends, E. J.; Ellis, D. E.; Ros, P. *Chem. Phys.* **1973**, *2*, 41.
- (23) Computer code ADF 2006.01: Baerends, E. J.; Autschbach, J.; Bérces, A.; Berger, J. A.; Bickelhaupt, F. M.; Bo, C.; de Boeijs, P. L.; Boerrigter, P. M.; Cavallo, L.; Chong, D. P.; Deng, L.; Dickson, R. M.; Ellis, D. E.; van Faassen, M.; Fan, L.; Fischer, T. H.; Fonseca Guerra, C.; van Gisbergen, S. J. A.; Groeneveld, J. A.; Gritsenko, O. V.; Grüning, M.; Harris, F. E.; van den Hoek, P.; Jacob, C. R.; Jacobsen, H.; Jensen, L.; Kadantsev, E. S.; van Kessel, G.; Klooster, R.; Kootstra, F.; van Lenthe, E.; McCormack, D. A.; Michalak, A.; Neugebauer, J.; Nicu, V. P.; Osinga, V. P.; Patchkovskii, S.; Philipsen, P. H. T.; Post, D.; Pye, C. C.; Ravenek, W.; Romaniello, P.; Ros, P.; Schipper, P. R. T.; Schreckenbach, G.; Snijders, J. G.; Solà, M.; Swart, M.; Swerhone, D.; te Velde, G.; Vernooijs, P.; Versluis, L.; Visscher, L.; Visser, O.; Wang, F.; Wesolowski, T. A.; van Wezenbeek, E. M.; Wiesenekker, G.; Wolff, S. K.; Woo, T. K.; Yakovlev, A. L.; Ziegler, T. *SCM: Theoretical Chemistry*, Vrije Universiteit: Amsterdam, The Netherlands, 2006.
- (24) Computer code AMBER 8: Case, D. A.; Darden, T. A.; Cheatham, T. E.; Simmerling, C. L.; Wang, J.; Duke, R. E.; Luo, R.; Merz, K. M.; Wang, B.; Pearlman, D. A.; Crowley, M.; Brozell, S.; Tsui, V.; Gohlke, H.; Mongan, J.; Hornak, V.; Cui, G.; Beroza, P.; Schafmeister, C.; Caldwell, J. W.; Ross, W. S.; Kollman P. A. University of California: San Francisco, 2004.
- (25) (a) Computer code QUILD (QUantum regions Interconnected by Local Description): Swart, M.; Bickelhaupt, F. M. Vrije Universiteit, Amsterdam, The Netherlands, 2006. (b) Swart, M.; Bickelhaupt, F. M. *J. Comput. Chem.* **2008**, *29*, online (DOI 10.1002/jcc.20834).
- (26) Swart, M.; Bickelhaupt, F. M. *Int. J. Quantum Chem.* **2006**, *106*, 2536.
- (27) Becke, A. D. *Phys. Rev. A* **1988**, *38*, 3098.
- (28) Perdew, J. P. *Phys. Rev. B* **1986**, *33*, 8822.
- (29) Swart, M.; Ehlers, A. W.; Lammertsma, K. *Mol. Phys.* **2004**, *102*, 2467.
- (30) Handy, N. C.; Cohen, A. J. *Mol. Phys.* **2001**, *99*, 403.
- (31) Perdew, J. P.; Burke, K.; Ernzerhof, M. *Phys. Rev. Lett.* **1996**, *77*, 3865.
- (32) Klamt, A.; Schüürmann, G. *J. Chem. Society., Perkin Trans. 2* **1993**, 799.
- (33) Klamt, A. *J. Phys. Chem.* **1995**, *99*, 2224.
- (34) Pye, C. C.; Ziegler, T. *Theor. Chem. Acc.* **1999**, *101*, 396.
- (35) Allinger, N. L.; Zhou, X. F.; Bergsma, J. *J. Mol. Struct. (THEOCHEM)* **1994**, *118*, 69.
- (36) Swart, M.; Rösler, E.; Bickelhaupt, F. M. *Eur. J. Inorg. Chem.* **2007**, 3646.
- (37) Swart, M.; van Duijnen, P. Th.; Snijders, J. G. *J. Comput. Chem.* **2001**, *22*, 79.
- (38) Cornell, W. D.; Cieplak, P.; Bayly, C. I.; Gould, I. R.; Merz, K. M.; Ferguson, D. M.; Spellmeyer, D. C.; Fox, T.; Caldwell, J. W.; Kollman, P. A. *J. Am. Chem. Soc.* **1995**, *117*, 5179.
- (39) Feller, S. E.; Zhang, Y. H.; Pastor, R. W.; Brooks, B. R. *J. Chem. Phys.* **1995**, *103*, 4613.
- (40) Darden, T.; York, D.; Pedersen, L. *J. Chem. Phys.* **1993**, *98*, 10089.
- (41) van der Wijst, T.; Fonseca Guerra, C.; Swart, M.; Bickelhaupt, F. M. *Chem. Phys. Lett.* **2006**, *426*, 415.
- (42) Fonseca Guerra, C.; Bickelhaupt, F. M.; Snijders, J. G.; Baerends, E. J. *J. Am. Chem. Soc.* **2000**, *122*, 4117.
- (43) van Bochove, M. A.; Bickelhaupt, F. M. *Eur. J. Org. Chem.* **2008**, 649.